

Geophysical Research Letters®



RESEARCH LETTER

10.1029/2024GL112711

Key Points:

- Satellite records reveal that almost half of the world's cities experienced changes in urban heat island (UHI) trends, mainly slowdowns
- The UHI deceleration occurs at a more rapid speed in larger cities and old urban area as compared to smaller cities and newly urbanized area
- The changes in UHI trends are intricately regulated by nonlinear changes in urbanization processes and background climate changes

Supporting Information:

Supporting Information may be found in the online version of this article.

Correspondence to:

L. Li,
longlinju@gmail.com






Citation:

Zhan, W., Li, L., Chakraborty, T. C., Hu, L., Wang, D., Liao, W., et al. (2025). Recent widespread deceleration of global surface urban heat islands unveiled by satellites. *Geophysical Research Letters*, 52, e2024GL112711. <https://doi.org/10.1029/2024GL112711>

Received 25 SEP 2024

Accepted 28 MAY 2025

Recent Widespread Deceleration of Global Surface Urban Heat Islands Unveiled by Satellites

Wenfeng Zhan^{1,2,3} , Long Li¹ , T. C. Chakraborty⁴, Leiqiu Hu⁵ , Dazhong Wang¹, Weilin Liao⁶ , Shasha Wang¹, Huilin Du¹, Fan Huang¹, Chunli Wang¹, Zihan Liu¹ , and Manchun Li⁷

¹Jiangsu Provincial Key Laboratory for Advanced Remote Sensing and Geographic Information Technology, International Institute for Earth System Science, Nanjing University, Nanjing, China, ²Jiangsu Center for Collaborative Innovation in Geographical Information Resource Development and Application, Nanjing, China, ³Frontiers Science Center for Critical Earth Material Cycling, Nanjing University, Nanjing, China, ⁴Pacific Northwest National Laboratory, Richland, WA, USA, ⁵Department of Atmospheric Science, University of Alabama in Huntsville, Huntsville, AL, USA, ⁶Guangdong Key Laboratory for Urbanization and Geo-Simulation, School of Geography and Planning, Sun Yat-sen University, Guangzhou, China, ⁷School of Geography and Ocean Science, Nanjing University, Nanjing, China

Abstract Tracking the temporal dynamics of urban heat island (UHI) is critical for urban heat adaptation and mitigation strategies. However, whether UHI trends have shifted recently and their underlying drivers remain unknown. Here we investigate the variabilities in surface UHI trends and their associated determinants in 2,104 cities worldwide from 2000 to 2022. Our findings reveal that approximately half of the world's cities have experienced notable shifts in surface UHI trends, predominantly characterized by UHI deceleration. These shifts can be primarily attributed to alterations in vegetation trends during the day and to modifications in surface albedo and local warming trends at night. Our study challenges the conventional linear models commonly employed to estimate surface UHI trends, suggesting potential biases in such estimates. Our findings underscore the need for nuanced policies to curtail UHI growth by considering changes in urban underlying surfaces and background climate, particularly from a nonlinear perspective.

Plain Language Summary Cities worldwide have witnessed a pervasive upward trend in surface urban heat island (UHI). However, it remains unclear whether this trend has changed. Here we reveal approximately half of the world's cities experiencing significant shifts in surface UHI trends, primarily characterized by deceleration. These shifts are mainly regulated by local changes in vegetation, albedo and air temperature. Our research underscores the limited understanding of temporal dynamics of surface UHI, offering the first indication of global prevalence of nonlinear trends. This implies that urban surface warming may not be as rapid as previously assumed in contrast to non-urban terrains. Our results also highlight the actionable potential of large-scale urban renewal initiatives to mitigate surface UHI.

1. Introduction

Cities confronting environmental and climate challenges are pivotal in advancing sustainable development (Esperon-Rodriguez et al., 2022; Grimm et al., 2008). Among these challenges is the urban heat island (UHI) effect, a phenomenon of cities experiencing elevated temperatures compared to their rural surroundings (Oke, 1973). Urban heat island can modify boundary layer dynamics, regional climate, and extreme weather events (Qian et al., 2022), thereby posing wide-ranging threats to environmental and public health (Hsu et al., 2021; Patz et al., 2005; X. Zhang et al., 2004). As urbanization and population growth continue, tracking the temporal UHI dynamics becomes critical for effective planning, assessing heat adaptation and mitigation strategies (He et al., 2022), and promoting sustainable urban development (UNEP, 2021).

The availability of high-quality satellite-based land surface temperature (LST) data has aided the tracking of surface UHI intensity (I_s , quantified by the difference between urban and rural LSTs) trends on a global scale (D. Zhou et al., 2019). Pioneering studies have predominantly employed linear diagnostic models to infer I_s trend (V_I , measured by the first derivative of I_s with time), implicitly assuming its constancy over time (Chakraborty & Lee, 2019; Si et al., 2022; Yao et al., 2019). These investigations generally revealed a rapid increase in I_s for most cities worldwide (L. Li, Zhan, Hu, et al., 2023; Z. Liu et al., 2022). However, case studies indicated substantial variability in V_I depending on the time frame (L. Li et al., 2022; Meng et al., 2018). For instance, the I_s exhibited

© 2025. The Author(s).

This is an open access article under the terms of the [Creative Commons Attribution-NonCommercial-NoDerivs](https://creativecommons.org/licenses/by/4.0/) License, which permits use and distribution in any medium, provided the original work is properly cited, the use is non-commercial and no modifications or adaptations are made.

an initial upward trend followed by a subsequent decline (i.e., deceleration) from 1988 to 2013 in Wuhan, China (Shen et al., 2016). Similarly, the urban agglomeration of the Greater Bay Area in China has experienced I_s deceleration since the 2000s (Feng et al., 2021). Consequently, interpreting the V_I using simple linear approaches may be invalid for cities with nonlinear V_I . Nonetheless, the prevalence of nonlinear V_I remains uncertain across global cities. Additionally, the information on acceleration, deceleration and constant rate in V_I can help to better characterize the interannual I_s variability from a non-linear perspective. Nevertheless, we lack information about the status of global cities with accelerating, decelerating, or stable V_I .

The major drivers of I_s comprise surface properties, climatic conditions, and human activities (Peng et al., 2012; D. Zhou et al., 2014). In the context of uneven urbanization (X. Liu et al., 2020) and climate change (Kosaka & Xie, 2013; Wei et al., 2021), alterations in any of these drivers may affect the variabilities in V_I . Investigating the underlying causes of the variabilities in V_I is critical for understanding how natural and anthropogenic drivers influence I_s in distinct urbanization phases (Feng et al., 2021; J. Li et al., 2021). While the impacts of these drivers on the I_s (Manoli et al., 2019; Zhao et al., 2014) and on the V_I (Chakraborty & Lee, 2019; Si et al., 2022; Yao et al., 2019) have been extensively studied on a large scale, their contribution to the variabilities in V_I (i.e., the second derivative of I_s with time), particularly across global cities, remains largely unexplored. Investigating the influencing factors of the variabilities in V_I helps to enhance the understanding of the causes of nonlinear I_s variations under climate change and urbanization. Therefore, there is a pressing need to understand the status and causes of the variabilities in V_I on a global scale.

To address these knowledge gaps, we investigate the recent (2000–2022) change rate of V_I (A_I , measured by the second derivative of I_s with time) across 2,104 global cities, using an extensive archive of satellite-derived LST estimates. We analyze the distribution of cities exhibiting distinct patterns of A_I . We further quantify the contributions of changes in surface properties, climatic conditions, and human activities to the observed A_I . Our study aims to advance the understanding of I_s dynamics, potentially helping to optimize urban planning and design in tackling urban heat islands.

2. Methods

2.1. Study Area and Data

Our study primarily focused on 2,104 cities worldwide with large urban areas. These cities are widely distributed in various climatic zones (Kottek et al., 2006). Detailed descriptions of the city selection procedures and distribution across different climate zones are provided in Text S1 in Supporting Information S1. We used several satellite-derived data sets to estimate the I_s , V_I and A_I , including LST, land cover type, elevation, and urban boundary. Additionally, we gathered data on the normalized difference vegetation index (NDVI), albedo, aerosol optical depth (AOD), surface air temperature, precipitation, population, and impervious surface to assist attribution analysis of the A_I . Further descriptions of these data sets are provided in Text S2 in Supporting Information S1.

2.2. Estimation of I_s , V_I , and A_I

Delineating urban and rural areas serves as the primary step for quantifying I_s , V_I , and A_I . The urban boundary is derived from the Global Urban Boundary (GUB) data set (L. Li et al., 2020; X. Li et al., 2020). A discussion of the choice of this GUB product over other urban boundary products is provided in the Text S3 in Supporting Information S1. We defined the urban surfaces as the pixels within the urban boundary in 2018 based on the latest available data. Analogous to previous studies (Liang et al., 2020; Yao et al., 2018), we further divided the urban surfaces into two urban subdivisions, that is, old urban area and newly urbanized area. The former subdivision was designated as the urban surfaces within the urban boundary in 1990, while the latter subdivision was outlined by the urban boundaries in 1990 and 2018. Note that the urban boundary in 1990 was only used to divide urban areas into two spatial units, rather than to emphasize the special significance of one specific year. It is also noted that when urban clusters are involved, several cities are sometimes represented within the boundaries of a single urban boundary (Bounoua et al., 2018). We defined the rural surroundings as a buffer of 1.5 times the urban area located outside the urban boundary in 2018. The incorporation of 1.5 times the urban areas for the rural reference rather than an equal size buffer allows for more pixels and suppresses the issues with too few pixels when examining small cities (Peng et al., 2012). To eliminate the influence of elevation and water bodies on the I_s estimation, we excluded the pixels labeled as water bodies, wetlands, and permanent snow and ice and the rural

pixels with an elevation exceeding ± 50 m above the mean urban elevation (Imhoff et al., 2010). The schematic outlining the categorization of urban and rural areas can be found in Figure S1 in Supporting Information S1.

We employed a segmented linear function-like approach (i.e., the moving window analysis at a decadal interval) to quantify the A_I across global cities between 2000 and 2022. This approach contains three major steps: (a) The I_s was first estimated as the difference between urban and rural LSTs. (b) The V_I was then calculated for 14 periods (i.e., 2000–2009, 2001–2010, ..., and 2013–2022) by 10-year moving window with 1-year step length based on yearly I_s . (c) A linear fitting was then performed for the calculated fourteen V_I values to obtain the A_I based on the slope of the linear fitting, and the A_I was finally tested for significance at the 0.05 level. To facilitate understanding of the methodology, we provide schematics to show the calculation process of A_I (Figure S2 in Supporting Information S1). Here the 10-year interval rather than shorter intervals was applied to avoid the inadequate number of data points within a certain period for linear fitting (F. Zhou et al., 2020). Such an approach avoids the incomparability across global cities due to differences in quantification criteria such as breakpoint number and segmentation period required in traditional segmented linear functions. The expressions of I_s , V_I , and A_I calculations are described as follows:

$$I_s = T_u - T_r \quad (1)$$

$$V_I = \frac{\Delta I_s}{\Delta t} \quad (2)$$

$$A_I = \frac{\Delta^2 I_s}{\Delta t^2} \quad (3)$$

where I_s denotes surface UHI intensity (unit: $^{\circ}\text{C}$); V_I denotes I_s trend (unit: $^{\circ}\text{C}/\text{decade}$); A_I represents the acceleration of I_s (unit: $^{\circ}\text{C}/\text{decade}^2$); T_u and T_r denote the urban (or old urban area and new urbanized area) and rural mean LSTs, respectively; t denotes time; “ Δ ” represents the mathematical symbol of difference; and “ 2 ” represents the mathematical symbol of second derivative.

For Equation 1, the I_s calculation was based on annual mean MODIS LST (March to February of the following year) mainly because we focus on the interannual I_s variation. Wherein, the LST data were produced with masked cloud and ocean pixels as well as poor input data. The mean LST error is within ± 0.6 K in most cases, which is much better than earlier products (Wan, 2014). Currently, MODIS LST data were widely used in studying surface UHI and its trend with good acceptance (Chakraborty & Lee, 2019; M. Yang et al., 2024). For Equation 2, the Δt equals to 10 years for calculating 14 V_I values, which was used to subsequently calculate the A_I . For Equation 3, the first Δt equals to 10 years and the second equals to 14 years for calculations when 10-year moving periods with 1-year nudges are implemented during the period 2000–2022. The cities are labeled as accelerated when $A_I > 0$, decelerated when $A_I < 0$, and stable when the A_I did not pass the significance test. The A_I was calculated for each city as well as using average I_s for a portion of selected cities.

It should be noted that the A_I estimates may be influenced by data and methodology. The Terra satellite suffers from orbital drift after 2020 and its data exhibit non-climatic discontinuities (Good et al., 2022). We therefore combined the Aqua MODIS data with a diurnal temperature cycle model (Hong et al., 2021) to correct for the effects of orbital drift, and assessed the reliability of Terra MODIS LST data. The analysis shows that the Terra MODIS LST data are still reliable in estimating I_s , V_I , and A_I (Text S4 in Supporting Information S1). The count of calculations for I_s in each year are different, which may represent different weights and therefore affect the A_I estimates. To validate this methodology, we divided the entire study period into two periods, 2000–2010 and 2012–2022 (i.e., it treats each year equally), and then calculated the A_I and compared it to the A_I values obtained by the methodology used in this study. The results show strong agreement between the two, demonstrating the reliability of the methodology in this study (Text S5 in Supporting Information S1).

2.3. Analysis of Regulators of A_I

We assembled NDVI, albedo, AOD, urban population, surface air temperature, and precipitation to examine the regulators of A_I . These studied factors jointly capture the key information on surface properties, background climate, and human activity that largely influence I_s (Cao et al., 2016; Lazzarini et al., 2015; Peng et al., 2012; Zhao et al., 2014). We then calculated the urban-rural differences in NDVI (δNDVI), albedo (δAlbedo), AOD

(δAOD), as well as urban population (POP), rural surface air temperature (TEMP), and rural precipitation (PRCP). Note that the parameters, including $\delta NDVI$, $\delta Albedo$, δAOD , and POP, are jointly influenced by urbanization and climate change, and it is therefore difficult to distinguish whether A_I is dominated by urbanization or climate change. Hence, we have chosen an indicator that is not disturbed by climate change to refer to urbanization, namely urban-rural difference in impervious surface percentage (δISP). Analogous to the A_I calculation, the 10-year moving window with 1-year step length was used to estimate the variabilities in the trends of these factors, namely the $\delta NDVI$ (denoted as $A_{\delta NDVI}$), $\delta Albedo$ ($A_{\delta Albedo}$), δAOD ($A_{\delta AOD}$), POP (A_{POP}), TEMP (A_{TEMP}), and PRCP (A_{PRCP}). Our analysis shows that there is no serious multicollinearity among these six factors and they are suitable for linear modeling because their variance inflation factors are less than 10 (Figure S3 in Supporting Information S1). We also used the same method to calculate $A_{\delta ISP}$ from δISP .

We further employed the geographically weighted regression (GWR) as well as ordinary least squares (OLS) to determine the relationship between the A_I and these factors across global cities. We compared GWR with OLS performances, and found the GWR outperforms the OLS with a better goodness of fit (R^2) (Table S1 in Supporting Information S1). We therefore used the GWR-fitted parameters to assess the contributions of these factors to A_I and to identify the most dominant factor for each city. We also constructed identical models to understand the relationship of A_I with urbanization (using $A_{\delta ISP}$) and climate change (using A_{TEMP} and A_{PRCP}). For a better comparison among various factors, we also quantified the relative contribution (in percentage) by the following equation (X. Liu et al., 2019):

$$P_i = \frac{|C_i|}{\sum |C_i|} \times 100\% \quad (4)$$

where P_i denotes the percent contribution of driver i ($i = A_{\delta NDVI}$, $A_{\delta Albedo}$, $A_{\delta AOD}$, A_{TEMP} , A_{PRCP} , and A_{POP}) to the A_I ; C_i denotes the contribution of driver i to the A_I , which was estimated by the GWR model. Here the absolute instead of the original values were used to calculate the percent contribution to avoid a single factor contributing $>100\%$ as well as to avoid the denominator being equal to zero.

3. Results

3.1. Spatiotemporal Patterns of A_I

Figure 1 shows that 48% of the world's cities during the day and 43% at night have statistically significant ($p < 0.05$, refer to Method) A_I . Among these, 34% of the cities exhibit significant I_s deceleration (i.e., $A_I < 0$) during the day, and those cities are widespread globally. Only 14% of the studied cities show significant I_s acceleration (i.e., $A_I > 0$), and they have been found to primarily cluster over central Eurasia (Figure 1a). There are 26% of the cities exhibiting significant I_s deceleration at night, while the percentage of cities with significant I_s acceleration is 17%, mainly located in Europe (Figure 1c).

The A_I exhibits remarkable spatial disparities across global cities. During the day, equatorial cities experience pronounced I_s deceleration, with a higher magnitude than in other climate zones (Figure 1b). At night, cities located in polar and snow zones exhibit the most notable I_s deceleration (Figure 1d). The A_I is negatively correlated with city size (Figures 1b and 1d), suggesting that I_s deceleration is more rapid in larger cities. This is potentially due to faster urban greening occurring in larger cities, as reported in a previous study (Sun et al., 2020).

The A_I values of different intra-city areas exhibit a strong correlation with each other (Figure S4 in Supporting Information S1). In addition, the A_I magnitude of old urban area generally exceeds that of newly urbanized area, with this disparity being insensitive to the specific year of urban boundary chosen for urban subdivisions (Figure S5 in Supporting Information S1). This suggests that although there are spatial differences in A_I values in different intra-city areas, A_I values are spatially highly correlated and they are larger in the old urban area than in the newly urbanized area. Therefore, our average outcomes (i.e., using urban boundaries in 2018) are typically lower than those in the old urban area and higher than those in the newly urbanized area, which reflects the average A_I in old urban area and newly urbanized area.

In addition, A_I also exhibits significant seasonal variations. During the daytime, I_s in spring and summer shows a more pronounced deceleration (i.e., $A_I < 0$), while during the nighttime, I_s in autumn and winter shows a more pronounced deceleration (Figure S6 in Supporting Information S1). Spatially, some European cities exhibit

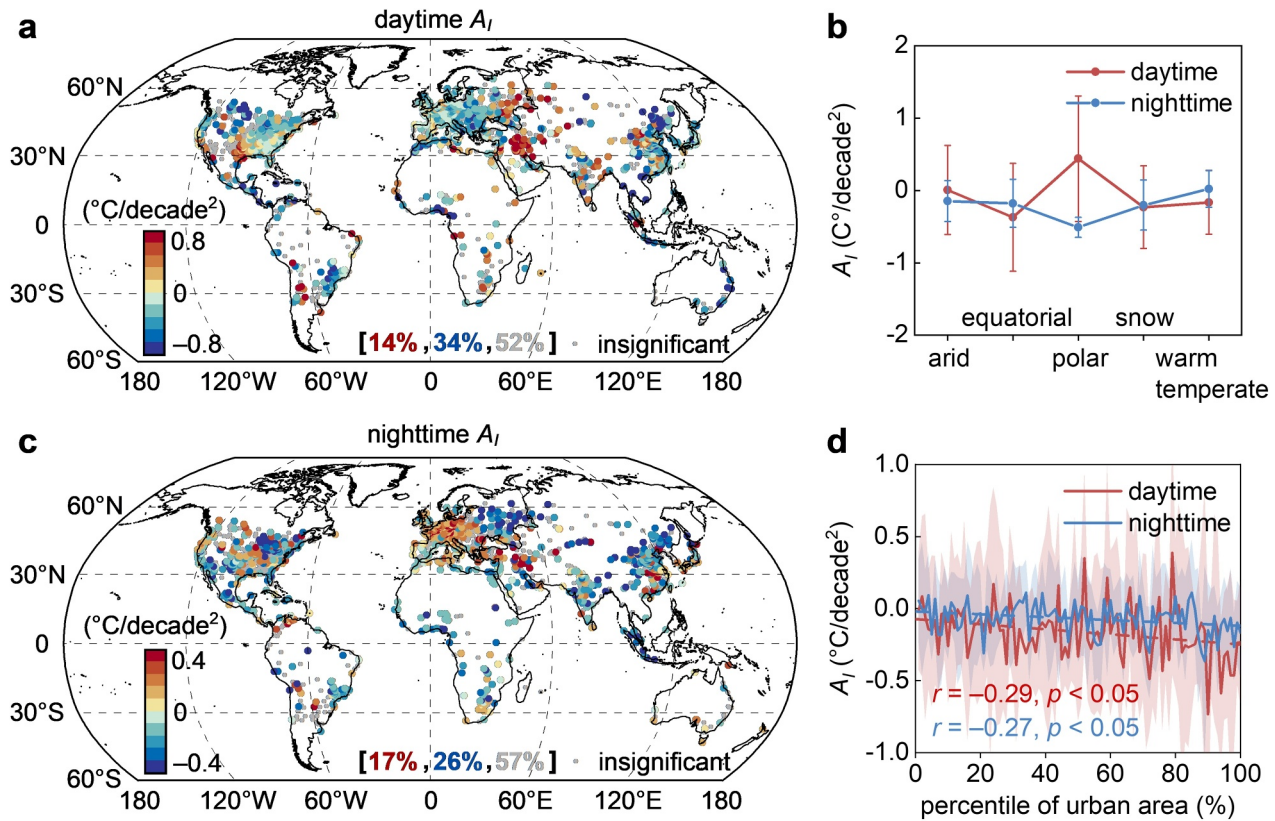


Figure 1. Spatial pattern of A_I and its variation with city size and climate zone over 2,104 cities worldwide for 2000–2022. Spatial pattern of A_I during the day (a). Mean A_I at each climate zone and the relationship between A_I and city size during the day (b). Panels (c, d), as in (a, b), but showing nighttime results corresponding to panels (a and b), respectively. The red and blue numbers in brackets in panels (a and c) indicate the percentages of cities with $A_I > 0$ (the accelerated V_I) and $A_I < 0$ (the decelerated V_I), respectively, with the percentages with underlines representing significant ($p < 0.05$), while the others denoting insignificant ($p > 0.05$). The relationships between A_I and city size in panels (b and d) are denoted based on sorting global cities by urban area through percentiles, with each percentile corresponding to an A_I mean (solid line) and standard deviation (shaded). The dots and bars of the climate zone-based summary in panels (b and d) represent the mean and standard deviation of the A_I , respectively.

contrasting features of accelerated I_s in summer and decelerated I_s in winter (Figure S7 in Supporting Information S1). These findings underscore the importance of considering climate zone, city size, urban subdivision, and seasonal variability when interpreting the A_I .

Figure 2 shows that the magnitude of I_s exhibits remarkable nonlinear variations for the cities with significant A_I . The mean I_s increases initially and then follows a stable or decreasing trend. Such a pattern of I_s changes is more noticeable when considering only cities with either accelerating I_s ($A_I > 0$) or decelerating I_s ($A_I < 0$). We also find that the V_I shows an approximately linear decrease (Figures 2a and 2c), with the daytime decrease faster than the nighttime decrease. From the first phase (2000–2010) to the second phase (2012–2022), the V_I decreases from 0.14°C/decade to −0.05°C/decade during the day, while it drops from 0.08°C/decade to 0.01°C/decade at night (Figures 2b and 2d). In addition, we observe slight differences in the mean A_I between different urban subdivisions (Figure S8 in Supporting Information S1), with the deceleration in the old urban area slightly more pronounced than that of the newly urbanized area both during the day and at night. These results indicate that the I_s has been decelerating in most cities since 2000, and the deceleration is even more rapid in the old urban area and during the day.

3.2. Divergent Impacts of Drivers on A_I

Figure 3 shows that the major drivers of the A_I in global cities differ between day and night. During the day, the A_I is mostly driven by the $A_{\delta NDVI}$ and $A_{\delta Albedo}$, with contributions being $42.5 \pm 25.6\%$ (mean \pm one standard deviation) and $17.8 \pm 19.9\%$, respectively (Figure 3a); and these two drivers are both negatively related to the A_I (Table S2 in Supporting Information S1). The $A_{\delta NDVI}$ is the dominant driver in most cities, while in mid- and high-

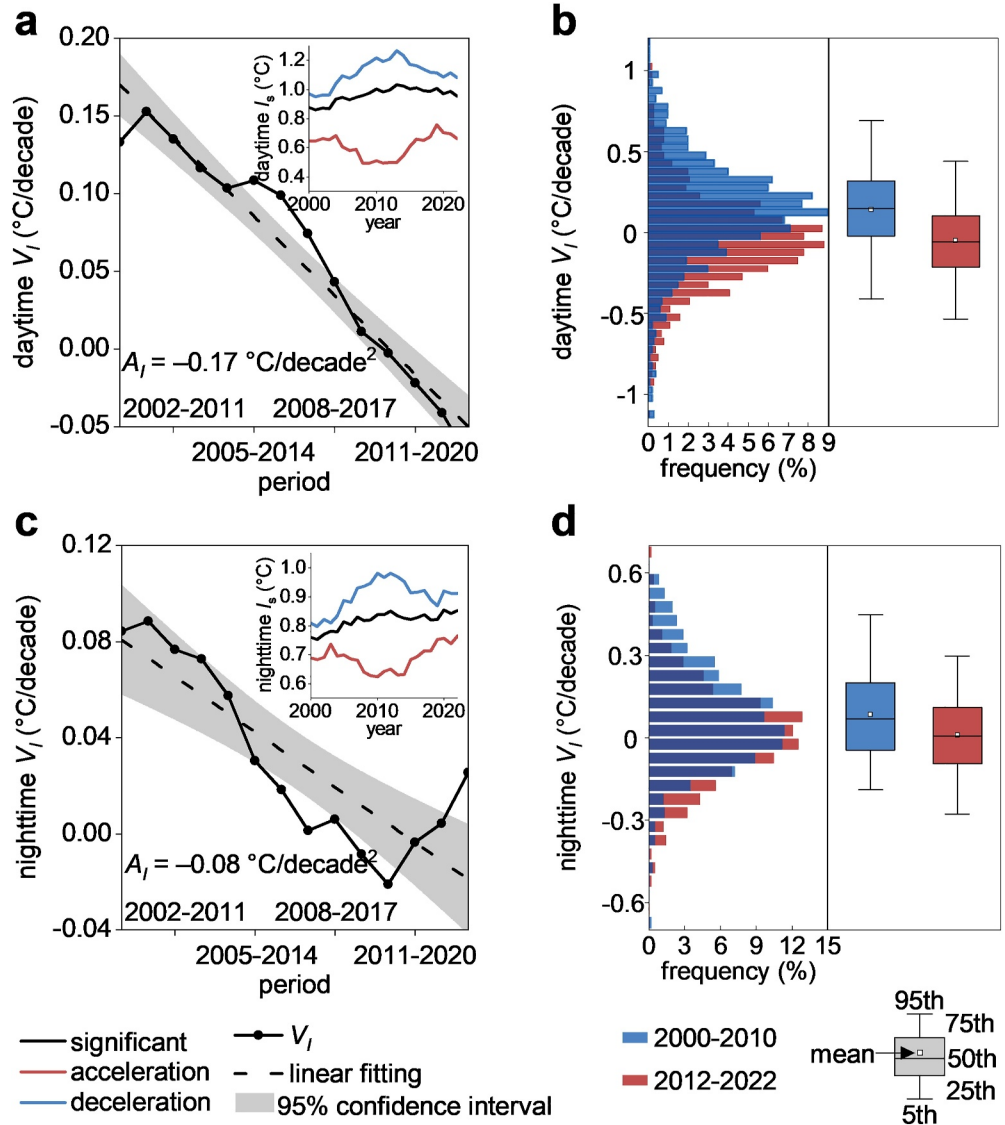


Figure 2. Temporal variations in I_s , V_I , and the A_I over all cities with significant A_I . Temporal variations in I_s , V_I , and the A_I during the day (a). The left panel shows the frequency distributions of daytime V_I across these cities between 2000–2010 and 2012–2022, while the right panel shows the boxplots of daytime V_I during these two periods (b). Panels (c, d), as in (a, b), but showing nighttime results corresponding to panels (a and b), respectively. In panels a and c, the red solid lines indicate the mean I_s variations; the red dot-dash lines indicate the mean I_s variations for all cities with $A_I > 0$; the red dotted lines indicate the I_s variations for all cities with $A_I < 0$; the black solid lines indicate the variations in the V_I ; the black dotted lines indicate the linear fit of the V_I (with the slope denoting the A_I); and the gray backgrounds indicate 95% confidence interval of the linear fit.

latitude cities in the Northern Hemisphere, the $A_{\delta\text{Albedo}}$ becomes the largest contributor (Figure 3a). At night, the $A_{\delta\text{Albedo}}$ and A_{TEMP} surpasses other factors in importance, and they contribute $26.6 \pm 24.0\%$ and $23.6 \pm 22.6\%$ to the A_I , respectively (Figure 3c). The A_I in North American and Central Eurasian cities is mostly controlled by the $A_{\delta\text{Albedo}}$. However, for cities along the west coast of North America and Western Europe, the A_{TEMP} can become the largest driver (Figure 3c). This is likely due to accelerated local warming over these regions (Figure S9 in Supporting Information S1). These results suggest that the A_I is mainly regulated by nonlinear changes in vegetation, albedo, temperature and precipitation. The important role of various drivers on A_I resembles the findings of previous studies focusing on I_s (L. Li et al., 2020; X. Li et al., 2020; Peng et al., 2012; D. Zhou et al., 2014). Considering the strong control of $A_{\delta\text{NDVI}}$ and $A_{\delta\text{Albedo}}$ on A_I , the spatial characteristics of their contributions are further elaborated in Text S6 in Supporting Information S1.

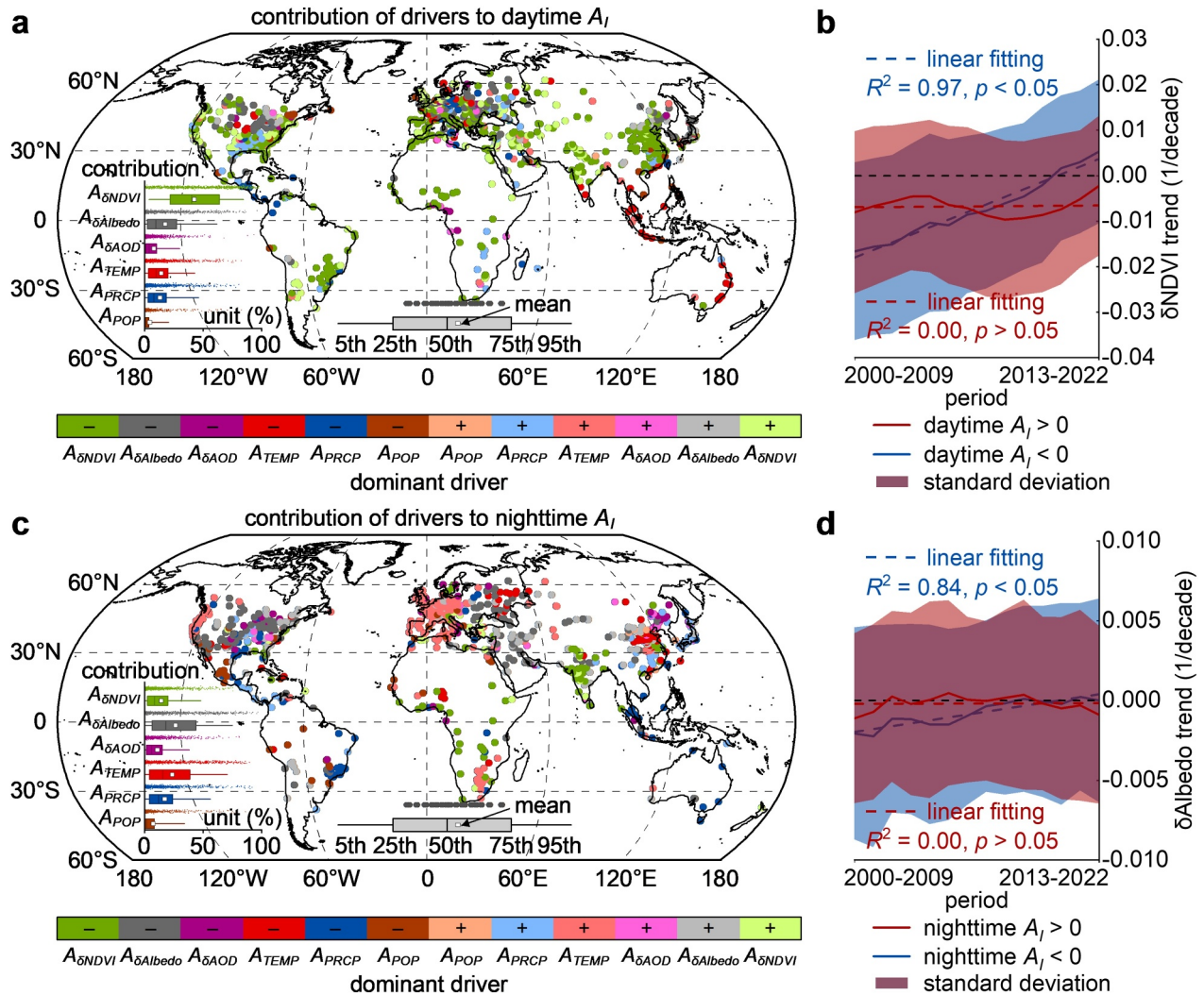


Figure 3. Dominant drivers of A_I across global cities. The most dominant drivers of A_I and their percentage contributions for each city during the day (a). Temporal variations of the urban-rural normalized difference vegetation index (NDVI) difference ($\delta NDMI$) for city categories with $A_I > 0$ and with $A_I < 0$ during the day (b). Panels (c, d), as in (a, b), but showing nighttime case and temporal variations of the urban-rural albedo difference ($\delta Albedo$) corresponding to panels (a and b), respectively. In panels (a and c), the “+” indicates a positive contribution to A_I , while “−” indicates a negative contribution. $A_{\delta NDMI}$, $A_{\delta Albedo}$, and $A_{\delta AOD}$ denote the second derivatives of the changes in urban-rural differences for NDVI, albedo, and aerosol optical depth, and A_{TEMP} , A_{PRCP} , and A_{POP} denote the second derivatives of the changes in rural surface air temperature (TEMP), precipitation (PRCP), and urban population (POP).

In cities with I_s deceleration (i.e., $A_I < 0$) during the day, the $\delta NDMI$ trend is negative around 2000 but it increases linearly and rapidly to around zero (i.e., $A_{\delta NDMI} > 0$; Figure 3b), while in cities with I_s deceleration at night, the $\delta Albedo$ trend is also negative and shows a significant linear increasing trend (Figure 3d). This indicates that the recent daytime I_s deceleration across most cities potentially results from the decelerated vegetation loss, while the nighttime I_s deceleration could be due to the decelerated reduction in albedo. For these cities, both urban and rural LSTs are accelerating, with the latter accelerating faster (Figure S10 in Supporting Information S1). In contrast, in cities with I_s acceleration (i.e., $A_I > 0$) during both the day and night, the $\delta NDMI$ and $\delta Albedo$ trends did not change significantly (Figures 3b and 3d). This implies that the I_s acceleration is likely to be significantly influenced by climate change and not solely dominated by surface properties when relative to that of I_s deceleration. For these cities, both urban and rural LSTs are accelerating, with the former accelerating faster (Figure S10 in Supporting Information S1). Overall, the recent I_s deceleration is mainly due to a slower rate of acceleration in urban LSTs than in rural areas, in the context of a general acceleration in LST growth globally (Figure S11 in Supporting Information S1). For the two urbanization subclasses considered here, we obtain similar

findings as described above (Figure S12 in Supporting Information S1). The relative contributions of urbanization and climate change to A_I are difficult to disentangle, since their impacts on δNDVI and δAlbedo are interdependent. Further analysis using $A_{\delta\text{ISP}}$, A_{TEMP} , and A_{PRCP} suggests that the A_I in Asia, Africa, and South America tended to be dominated by urbanization, while climate change had a stronger impact in Europe and eastern North America, with significant differences across climate zones (Figure S13 in Supporting Information S1).

4. Discussion and Implications

Accurately tracking UHI trends is critical to understanding the changing environmental impacts resulting from urbanization and climate change. Traditional ground-based observations are valuable for monitoring UHI trends (Wang & Shu, 2020; L. Zhang et al., 2024). However, accurate monitoring of global UHI trends using such measurements remains challenging, in part due to their limited presence within highly heterogeneous urban environments (Du et al., 2021; Y. Yang et al., 2020). The recent emergence of crowd-sourced meteorological data offers a potential solution to alleviate this intra-city heterogeneity issue (Venter et al., 2021). Nevertheless, the widespread availability of such densely distributed data is a very recent development, making such data less suitable for monitoring long-term UHI trends. Another notable challenge is the extremely uneven global distribution of ground-based meteorological observations (J. Li et al., 2023). This disadvantage severely hampers the global monitoring of UHI trends by site-based meteorological measurements, especially in the Global South. Furthermore, numerical climate models still face challenges in accurately identifying long-term UHI trends, especially at fine resolutions, due to their inherently simplified parameterization of urban surface-atmosphere interactions and computational bottlenecks (Qian et al., 2022).

Satellite-derived LST products appear to be the critical approach for detecting UHI trends at the city-specific level worldwide as well as at the granular level (Lee & Dessler, 2024; Voogt & Oke, 2003). With the accumulation of satellite LST data, a growing body of studies have revealed surface UHI (I_s) trends worldwide, suggesting that most cities are experiencing rapid I_s growth (Chakraborty & Lee, 2019; L. Li, Zhan, Hu, et al., 2023; Z. Liu et al., 2022; Si et al., 2022; Yao et al., 2019). However, these studies have predominately examined V_I based on a simple linear assumption. This linear approach may become invalid and introduce biases in projections, especially when cities exhibit nonlinear V_I due to rapid urbanization and climate change (Feng et al., 2021). Using a comprehensive archive of satellite LST data, our study shows that over 40% of the world's cities have witnessed significant shifts in V_I since 2000, with most of them displaying I_s deceleration (Figures 1 and 2).

To the best of our knowledge, our study offers the first indication of the global prevalence of nonlinear V_I , suggesting that the use of simple linear models can yield biased estimates in V_I . Moreover, this suggests that urban surface warming may not be as rapid as extrapolated from linear models, particularly over cities that experience I_s deceleration. This aligns with previous multi-model projections of global urban climates, especially under high-emission scenarios (Zhao et al., 2021), albeit with distinctions in skin-surface or surface-air temperatures in quantification.

The widespread I_s deceleration appears optimistic as it signifies that UHI may not continually intensify and, as a result, the urbanization-induced extra heat stress may not amplify incessantly. However, it becomes pessimistic when considering a warmer future. Adding 0.5°C of UHI (i.e., additional urban warmth) to a hotter period has a markedly different impact on extreme heat events when compared to adding it to a colder period—the combination of a warmer phase and additional urban warmth can lead to more frequent and severe heatwaves (Hansen et al., 2012). In addition, despite widespread I_s deceleration, UHI footprint continues to expand with city size and population (Hu et al., 2022), exposing a larger population to extra urban warmth. This emphasizes the necessity of combining UHI intensity and footprint when assessing the impact of urban warming on residents. Simultaneously, population dynamics can also modify the exposure of urban residents to extra urban warmth, thus requiring additional consideration within urban climate adaptation strategies (J. Yang et al., 2019). Furthermore, our study may provide implications for canopy UHI, given the similar spatiotemporal patterns between surface and canopy UHI at night (Du et al., 2021; Venter et al., 2021). The widespread nighttime I_s deceleration and even reductions in I_s magnitude at night in certain cities caution against relying on superlinear scaling relationships between UHI intensity and city population, commonly accepted in urban climatology (Oke et al., 2017). However, it should also be noted that the design of urban heat adaptation and mitigation strategies may not be based solely on the UHI intensity (Martilli et al., 2020) or LST (Parlow, 2021).

Our results show that the I_s deceleration is more pronounced in larger cities and old urban area as compared to smaller cities and newly urbanized area (Figure 1 and Figure S8 in Supporting Information S1). This indicates that highly urbanized regions are more likely to experience I_s deceleration. For instance, some old urban areas of megacity (e.g., Beijing and Shanghai) have experienced slight decreases in I_s magnitudes in recent years (L. Li et al., 2022). Our study demonstrates that the shift from positive to negative V_f in old urban area should be attributable to substantial greening (Figure S12 in Supporting Information S1) initiated by both biogeochemical factors (L. Li, Zhan, Ju, et al., 2023) and urban renewal activities (Jin et al., 2018; J. Li et al., 2021), resonating with the well-documented cooling impact of urban tree cover (Schwaab et al., 2021). In general, regulating biogeochemical drivers may pose challenges, while our empirical evidence in individual cities suggests that large-scale urban renewal endeavors can effectively mitigate local I_s growth (Figure S14 in Supporting Information S1). This highlights the actionable feasibility of employing such urban renewal endeavors to curtail V_f and to achieve greater benefits over old urban area of megacity characterized by strong I_s and high population density. Nonetheless, it is also essential to underscore that urban renewal endeavors can achieve greater cooling benefits through a more targeted focus on underprivileged communities, thus redressing the existing disparity in access to green space cooling (W. Zhou et al., 2021) and optimizing financial resources allocation (Ziter et al., 2019). Our results also show that cities with I_s acceleration (Figure 1, e.g., arid and European cities) are primarily controlled by climate change, with surface properties exerting relatively fewer influences (Figure 3 and Figure S15 in Supporting Information S1). This emphasizes the need to integrate climate change impacts into heat adaptation and mitigation strategies in such cities. We acknowledge several limitations of our study, including timespan, difficulty in detecting second-order signals, land surface observation, missing data resulting from cloud contamination, and attribution method. Elaborate discussions on these limitations are provided in Text S7 in Supporting Information S1.

Conflict of Interest

The authors declare no conflicts of interest relevant to this study.

Data Availability Statement

All data used in this study are publicly available online. The MODIS LST product (MOD11A1) is available at https://developers.google.cn/earth-engine/datasets/catalog/MODIS_061_MOD11A1 (Wan et al., 2021). The MODIS land cover type product (MCD12Q1) is available at https://developers.google.cn/earth-engine/datasets/catalog/MODIS_061_MCD12Q1 (Friedl & Sulla-Menasse, 2022). The MODIS NDVI product (MOD13A2) is available at https://developers.google.cn/earth-engine/datasets/catalog/MODIS_061_MOD13A2 (Didan, 2021). The MODIS albedo product (MCD43A3) is available at https://developers.google.cn/earth-engine/datasets/catalog/MODIS_061_MCD43A3 (Schaaf & Wang, 2021). The MODIS AOD product (MCD19A2) is available at https://developers.google.cn/earth-engine/datasets/catalog/MODIS_061_MCD19A2_GRANULES (Lyapustin & Wang, 2022). The Shuttle Radar Topography Mission (SRTM) digital elevation model can be downloaded at <https://srtm.csi.cgiar.org/> (Reuter et al., 2007). The GUB data can be downloaded at <http://data.starcloud.pcl.ac.cn/zh/resource/14> (L. Li et al., 2020; X. Li et al., 2020). The surface air temperature and precipitation data can be downloaded at https://psl.noaa.gov/data/gridded/data.UDel_AirT_Precip.html (Matsuura & Willmott, 2018). The population data can be downloaded at <http://data.europa.eu/89h/d6d86a90-4351-4508-99c1-cb074b022c4a> (Schiavina et al., 2022).

References

- Bounoua, L., Nigro, J., Zhang, P., Thome, K., & Lachir, A. (2018). Mapping urbanization in the United States from 2001 to 2011. *Applied Geography*, 90, 123–133. <https://doi.org/10.1016/j.apgeog.2017.12.002>
- Cao, C., Lee, X., Liu, S., Schultz, N., Xiao, W., Zhang, M., & Zhao, L. (2016). Urban heat islands in China enhanced by haze pollution. *Nature Communications*, 7, 1–7. <https://doi.org/10.1038/ncomms12509>
- Chakraborty, T., & Lee, X. (2019). A simplified urban-extent algorithm to characterize surface urban heat islands on a global scale and examine vegetation control on their spatiotemporal variability. *International Journal of Applied Earth Observation and Geoinformation*, 74, 269–280. <https://doi.org/10.1016/j.jag.2018.09.015>
- Didan, K. (2021). MODIS/Terra Vegetation Indices 16-Day L3 Global 1km SIN Grid V061 [Dataset]. *NASA EOSDIS Land Processes Distributed Active Archive Center*. <https://doi.org/10.5067/MODIS/MOD13A2.061>
- Du, H., Zhan, W., Liu, Z., Li, J., Li, L., Lai, J., et al. (2021). Simultaneous investigation of surface and canopy urban heat islands over global cities. *ISPRS Journal of Photogrammetry and Remote Sensing*, 181, 67–83. <https://doi.org/10.1016/j.isprsjprs.2021.09.003>
- Esperon-Rodriguez, M., Tjoelker, M. G., Lenoir, J., Baumgartner, J. B., Beaumont, L. J., Nipperess, D. A., et al. (2022). Climate change increases global risk to urban forests. *Nature Climate Change*, 12(10), 950–955. <https://doi.org/10.1038/s41558-022-01465-8>

Acknowledgments

We gratefully acknowledge the following organizations for providing the funding to support this study, including the National Natural Science Foundation of China (Grant 42171306), Fundamental Research Funds for the Central Universities (Grant 2024300388), and 'GeoX' Interdisciplinary Project of Frontiers Science Center for Critical Earth Material Cycling (Grant 20250209). We also thank the support from the National Youth Talent Support Program of China. Pacific Northwest National Laboratory is operated for the U.S. Department of Energy (DOE) by Battelle Memorial Institute under contract DE-AC05-76RL01830. T.C.'s contribution was supported by a DOE Early Career Research Program grant, and the Coastal Observations, Mechanisms, and Predictions Across Systems and Scales-Great Lakes Modeling (COMPASS-GLM) and Integrated Coastal Modeling (ICoM) projects.

- Feng, R., Wang, F., Wang, K., Wang, H., & Li, L. (2021). Urban ecological land and natural-anthropogenic environment interactively drive surface urban heat island: An urban agglomeration-level study in China. *Environment International*, 157, 106857. <https://doi.org/10.1016/j.envint.2021.106857>
- Friedl, M., & Sulla-Menashé, D. (2022). MODIS/Terra+Aqua Land Cover Type Yearly L3 Global 500m SIN Grid V061 [Dataset]. NASA EOSDIS Land Processes Distributed Active Archive Center. <https://doi.org/10.5067/MODIS/MCD12Q1.061>
- Good, E. J., Aldred, F. M., Ghent, D. J., Veal, K. L., & Jimenez, C. (2022). An analysis of the stability and trends in the LST_cci land surface temperature datasets over Europe. *Earth and Space Science*, 9, e2022EA002317. <https://doi.org/10.1029/2022EA002317>
- Grimm, N. B., Faeth, S. H., Golubiewski, N. E., Redman, C. L., Wu, J., Bai, X., & Briggs, J. M. (2008). Global change and the ecology of cities. *Science*, 319(5864), 756–760. <https://doi.org/10.1126/science.1150195>
- Hansen, J., Sato, M., & Ruedy, R. (2012). Perception of climate change. *Proceedings of the National Academy of Sciences*, 109(37), E2415–E2423. <https://doi.org/10.1073/pnas.1205276109>
- He, C., Zhang, Y., Schneider, A., Chen, R., Zhang, Y., Ma, W., et al. (2022). The inequality labor loss risk from future urban warming and adaptation strategies. *Nature Communications*, 13(1), 3847. <https://doi.org/10.1038/s41467-022-31145-2>
- Hong, F., Zhan, W., Göttsche, F. M., Lai, J., Liu, Z., Hu, L., et al. (2021). A simple yet robust framework to estimate accurate daily mean land surface temperature from thermal observations of tandem polar orbiters. *Remote Sensing of Environment*, 264, 112612. <https://doi.org/10.1016/j.rse.2021.112612>
- Hsu, A., Sheriff, G., Chakraborty, T., & Manya, D. (2021). Disproportionate exposure to urban heat island intensity across major US cities. *Nature Communications*, 12(1), 2721. <https://doi.org/10.1038/s41467-021-22799-5>
- Hu, J., Yang, Y., Zhou, Y., Zhang, T., Ma, Z., & Meng, X. (2022). Spatial patterns and temporal variations of footprint and intensity of surface urban heat island in 141 China cities. *Sustainable Cities and Society*, 77, 103585. <https://doi.org/10.1016/j.scs.2021.103585>
- Imhoff, M. L., Zhang, P., Wolfe, R. E., & Bounoua, L. (2010). Remote sensing of the urban heat island effect across biomes in the continental USA. *Remote Sensing of Environment*, 114(3), 504–513. <https://doi.org/10.1016/j.rse.2009.10.008>
- Jin, C., Bai, X., Luo, T., & Zou, M. (2018). Effects of green roofs' variations on the regional thermal environment using measurements and simulations in Chongqing, China. *Urban Forestry & Urban Greening*, 29, 223–237. <https://doi.org/10.1016/j.ufug.2017.12.002>
- Kosaka, Y., & Xie, S. P. (2013). Recent global-warming hiatus tied to equatorial Pacific surface cooling. *Nature*, 501(7467), 403–407. <https://doi.org/10.1038/nature12534>
- Kottek, M., Grieser, J., Beck, C., Rudolf, B., & Rubel, F. (2006). World map of the Köppen-Geiger climate classification updated. *Meteorologische Zeitschrift*, 15(3), 259–263. <https://doi.org/10.1127/0941-2948/2006/0130>
- Lazzarini, M., Molini, A., Marpu, P. R., Ouarda, T. B., & Ghedira, H. (2015). Urban climate modifications in hot desert cities: The role of land cover, local climate, and seasonality. *Geophysical Research Letters*, 42(22), 9980–9989. <https://doi.org/10.1002/2015GL066534>
- Lee, J., & Dessler, A. E. (2024). Improved surface urban heat impact assessment using GOES satellite data: A comparative study with ERA-5. *Geophysical Research Letters*, 51(1), e2023GL107364. <https://doi.org/10.1029/2023GL107364>
- Li, J., Zhan, W., Chakraborty, T. C., Liu, Z., Du, H., Liao, W., et al. (2023). Satellite-based ranking of the world's hottest and coldest cities reveals inequitable distribution of temperature extremes. *Bulletin of the American Meteorological Society*, 104(7), E1268–E1281. <https://doi.org/10.1175/BAMS-D-22-0233.1>
- Li, J., Zhan, W., Hong, F., Lai, J., Dong, P., Liu, Z., et al. (2021). Similarities and disparities in urban local heat islands responsive to regular-stable-and counter-urbanization: A case study of Guangzhou, China. *Building and Environment*, 199, 107935. <https://doi.org/10.1016/j.buildenv.2021.107935>
- Li, L., Zha, Y., & Zhang, J. (2020). Spatially non-stationary effect of underlying driving factors on surface urban heat islands in global major cities. *International Journal of Applied Earth Observation and Geoinformation*, 90, 102131. <https://doi.org/10.1016/j.jag.2020.102131>
- Li, L., Zhan, W., Du, H., Lai, J., Wang, C., Fu, H., et al. (2022). Long-term and fine-scale surface urban heat island dynamics revealed by Landsat data since the 1980s: A comparison of four megacities in China. *Journal of Geophysical Research: Atmospheres*, 127(5), e2021JD035598. <https://doi.org/10.1029/2021JD035598>
- Li, L., Zhan, W., Hu, L., Chakraborty, T. C., Wang, Z., Fu, P., et al. (2023). Divergent urbanization-induced impacts on global surface urban heat island trends since 1980s. *Remote Sensing of Environment*, 295, 113650. <https://doi.org/10.1016/j.rse.2023.113650>
- Li, L., Zhan, W., Ju, W., Peñuelas, J., Zhu, Z., Peng, S., et al. (2023). Competition between biogeochemical drivers and land-cover changes determines urban greening or browning. *Remote Sensing of Environment*, 287, 113481. <https://doi.org/10.1016/j.rse.2023.113481>
- Li, X., Gong, P., Zhou, Y., Wang, J., Bai, Y., Chen, B., et al. (2020). Mapping global urban boundaries from the global artificial impervious area (GAIA) data. *Environmental Research Letters*, 15(9), 094044. <https://doi.org/10.1088/1748-9326/ab9be3>
- Liang, Z., Wu, S., Wang, Y., Wei, F., Huang, J., Shen, J., & Li, S. (2020). The relationship between urban form and heat island intensity along the urban development gradients. *Science of the Total Environment*, 708, 135011. <https://doi.org/10.1016/j.scitotenv.2019.135011>
- Liu, X., Huang, Y., Xu, X., Li, X., Li, X., Ciais, P., et al. (2020). High-spatiotemporal-resolution mapping of global urban change from 1985 to 2015. *Nature Sustainability*, 3(7), 564–570. <https://doi.org/10.1038/s41893-020-0521-x>
- Liu, X., Pei, F., Wen, Y., Li, X., Wang, S., Wu, C., et al. (2019). Global urban expansion offsets climate-driven increases in terrestrial net primary productivity. *Nature Communications*, 10, 1–8. <https://doi.org/10.1038/s41467-019-13462-1>
- Liu, Z., Zhan, W., Bechtel, B., Voogt, J., Lai, J., Chakraborty, T., et al. (2022). Surface warming in global cities is substantially more rapid than in rural background areas. *Communications Earth & Environment*, 3(1), 219. <https://doi.org/10.1038/s43247-022-00539-x>
- Lyapustin, A., & Wang, Y. (2022). MODIS/Terra+Aqua Land Aerosol Optical Depth Daily L2G Global 1km SIN Grid V061 [Dataset]. NASA EOSDIS Land Processes Distributed Active Archive Center. <https://doi.org/10.5067/MODIS/MCD19A2.061>
- Manoli, G., Faticchi, S., Schläpfer, M., Yu, K., Crowther, T. W., Meili, N., et al. (2019). Magnitude of urban heat islands largely explained by climate and population. *Nature*, 573(7772), 55–60. <https://doi.org/10.1038/s41586-019-1512-9>
- Martilli, A., Krayenhoff, E. S., & Nazarian, N. (2020). Is the Urban Heat Island intensity relevant for heat mitigation studies? *Urban Climate*, 31, 100541. <https://doi.org/10.1016/j.uclim.2019.100541>
- Matsuura, K., & Willmott, C. J. (2018). Terrestrial precipitation: 1900–2017 gridded monthly time series [Dataset]. Electronic. *Department of Geography, University of Delaware*. https://psl.noaa.gov/data/gridded/data.UDel_AirT_Precip.html.19716.
- Meng, Q., Zhang, L., Sun, Z., Meng, F., Wang, L., Sun, Y., et al. (2018). Characterizing spatial and temporal trends of surface urban heat island effect in an urban main built-up area: A 12-year case study in Beijing, China. *Remote Sensing of Environment*, 204, 826–837. <https://doi.org/10.1016/j.rse.2017.09.019>
- Oke, T. R. (1973). City size and the urban heat island. *Atmospheric Environment*, 7(8), 769–779. [https://doi.org/10.1016/0004-6981\(73\)90140-6](https://doi.org/10.1016/0004-6981(73)90140-6)
- Oke, T. R., Mills, G., Christen, A., & Voogt, J. A. (2017). *Urban climates*. Cambridge University Press. <https://doi.org/10.1017/9781139016476>
- Parlow, E. (2021). Regarding some pitfalls in urban heat island studies using remote sensing technology. *Remote Sensing*, 13(18), 3598. <https://doi.org/10.3390/rs13183598>

- Patz, J. A., Campbell-Lendrum, D., Holloway, T., & Foley, J. A. (2005). Impact of regional climate change on human health. *Nature*, 438(7066), 310–317. <https://doi.org/10.1038/nature04188>
- Peng, S., Piao, S., Ciais, P., Friedlingstein, P., Ottle, C., Bréon, F. M., et al. (2012). Surface urban heat island across 419 global big cities. *Environmental Science & Technology*, 46(2), 696–703. <https://doi.org/10.1021/es2030438>
- Qian, Y., Chakraborty, T. C., Li, J., Li, D., He, C., Sarangi, C., et al. (2022). Urbanization impact on regional climate and extreme weather: Current understanding, uncertainties, and future research directions. *Advances in Atmospheric Sciences*, 39(6), 819–860. <https://doi.org/10.1007/s00376-021-1371-9>
- Reuter, H. I., Nelson, A., & Jarvis, A. (2007). An evaluation of void-filling interpolation methods for SRTM data. *International Journal of Geographical Information Science*, 21(9), 983–1008. <https://doi.org/10.1080/13658810601169899>
- Schaaf, C., & Wang, Z. (2021). MODIS/Terra+Quia BRDF/Albedo Daily L3 Global - 500m V061 [Dataset]. NASA EOSDIS Land Processes Distributed Active Archive Center. <https://doi.org/10.5067/MODIS/MCD43A3.061>
- Schiavina, M., Freire, S., & MacManus, K. (2022). GHS-POP R2022A - GHS population grid multitemporal (1975-2030) - OBSOLETE RELEASE [Dataset]. European Commission, Joint Research Centre (JRC). <https://doi.org/10.2905/D6D86A90-4351-4508-99C1-CB074B022C4A>
- Schwaab, J., Meier, R., Mussetti, G., Seneviratne, S., Bürgi, C., & Davin, E. L. (2021). The role of urban trees in reducing land surface temperatures in European cities. *Nature Communications*, 12(1), 6763. <https://doi.org/10.1038/s41467-021-26768-w>
- Shen, H., Huang, L., Zhang, L., Wu, P., & Zeng, C. (2016). Long-term and fine-scale satellite monitoring of the urban heat island effect by the fusion of multi-temporal and multi-sensor remote sensed data: A 26-year case study of the city of Wuhan in China. *Remote Sensing of Environment*, 172, 109–125. <https://doi.org/10.1016/j.rse.2015.11.005>
- Si, M., Li, Z. L., Nerry, F., Tang, B. H., Leng, P., Wu, H., et al. (2022). Spatiotemporal pattern and long-term trend of global surface urban heat islands characterized by dynamic urban-extent method and MODIS data. *ISPRS Journal of Photogrammetry and Remote Sensing*, 183, 321–335. <https://doi.org/10.1016/j.isprsjprs.2021.11.017>
- Sun, L., Chen, J., Li, Q., & Huang, D. (2020). Dramatic uneven urbanization of large cities throughout the world in recent decades. *Nature Communications*, 11, 1–9. <https://doi.org/10.1038/s41467-020-19158-1>
- UNEP. (2021). *Beating the heat: A sustainable cooling handbook for cities*. United Nations Environment Programme. Retrieved from <https://lib.icimod.org/record/35640>
- Venter, Z. S., Chakraborty, T., & Lee, X. (2021). Crowdsourced air temperatures contrast satellite measures of the urban heat island and its mechanisms. *Science Advances*, 7(22), eabb9569. <https://doi.org/10.1126/sciadv.abb9569>
- Voogt, J. A., & Oke, T. R. (2003). Thermal remote sensing of urban climates. *Remote Sensing of Environment*, 86(3), 370–384. [https://doi.org/10.1016/S0034-4257\(03\)00079-8](https://doi.org/10.1016/S0034-4257(03)00079-8)
- Wan, Z. (2014). New refinements and validation of the collection-6 MODIS land-surface temperature/emissivity product. *Remote Sensing of Environment*, 140, 36–45. <https://doi.org/10.1016/j.rse.2006.06.026>
- Wan, Z., Hook, S., & Hulley, G. (2021). MODIS/Terra Land Surface Temperature/Emissivity Daily L3 Global 1km SIN Grid V061 [Dataset]. NASA EOSDIS Land Processes Distributed Active Archive Center. <https://doi.org/10.5067/MODIS/MOD11A1.061>
- Wang, W., & Shu, J. (2020). Urban renewal can mitigate urban heat islands. *Geophysical Research Letters*, 47(6), e2019GL085948. <https://doi.org/10.1029/2019GL085948>
- Wei, J., Li, Z., Lyapustin, A., Sun, L., Peng, Y., Xue, W., et al. (2021). Reconstructing 1-km-resolution high-quality PM_{2.5} data records from 2000 to 2018 in China: Spatiotemporal variations and policy implications. *Remote Sensing of Environment*, 252, 112136. <https://doi.org/10.1016/j.rse.2020.112136>
- Yang, J., Hu, L., & Wang, C. (2019). Population dynamics modify urban residents' exposure to extreme temperatures across the United States. *Science Advances*, 5(12), eaay3452. <https://doi.org/10.1126/sciadv.aay3452>
- Yang, M., Ren, C., Wang, H., Wang, J., Feng, Z., Kumar, P., et al. (2024). Mitigating urban heat island through neighboring rural land cover. *Nature Cities*, 1(8), 1–11. <https://doi.org/10.1038/s44284-024-00091-z>
- Yang, Y., Zheng, Z., Yim, S. Y., Roth, M., Ren, G., Gao, Z., et al. (2020). PM_{2.5} pollution modulates wintertime urban heat island intensity in the Beijing-Tianjin-Hebei Megalopolis, China. *Geophysical Research Letters*, 47(1), e2019GL084288. <https://doi.org/10.1029/2019GL084288>
- Yao, R., Wang, L., Huang, X., Gong, W., & Xia, X. (2019). Greening in rural areas increases the surface urban heat island intensity. *Geophysical Research Letters*, 46(4), 2204–2212. <https://doi.org/10.1029/2018GL081816>
- Yao, R., Wang, L., Huang, X., Zhang, W., Li, J., & Niu, Z. (2018). Interannual variations in surface urban heat island intensity and associated drivers in China. *Journal of Environmental Management*, 222, 86–94. <https://doi.org/10.1016/j.jenvman.2018.05.024>
- Zhang, L., Luo, F., Pan, G., Zhang, W., Ren, G., Zheng, Z., & Yang, Y. (2024). Elucidating the multi-timescale variability of a canopy urban heat island by using the short-time Fourier transform. *Geophysical Research Letters*, 51(1), e2023GL106221. <https://doi.org/10.1029/2023GL106221>
- Zhang, X., Friedl, M. A., Schaaf, C. B., Strahler, A. H., & Schneider, A. (2004). The footprint of urban climates on vegetation phenology. *Geophysical Research Letters*, 31(12), L12209. <https://doi.org/10.1029/2004GL020137>
- Zhao, L., Lee, X., Smith, R. B., & Oleson, K. (2014). Strong contributions of local background climate to urban heat islands. *Nature*, 511(7508), 216–219. <https://doi.org/10.1038/nature13462>
- Zhao, L., Oleson, K., Bou-Zeid, E., Krayenhoff, E. S., Bray, A., Zhu, Q., et al. (2021). Global multi-model projections of local urban climates. *Nature Climate Change*, 11(2), 152–157. <https://doi.org/10.1038/s41558-020-00958-8>
- Zhou, D., Xiao, J., Bonafoni, S., Berger, C., Deilami, K., Zhou, Y., et al. (2019). Satellite remote sensing of surface urban heat islands: Progress, challenges, and perspectives. *Remote Sensing*, 11(1), 48. <https://doi.org/10.3390/rs11010048>
- Zhou, D., Zhao, S., Liu, S., Zhang, L., & Zhu, C. (2014). Surface urban heat island in China's 32 major cities: Spatial patterns and drivers. *Remote Sensing of Environment*, 152, 51–61. <https://doi.org/10.1016/j.rse.2014.05.017>
- Zhou, F., Bo, Y., Ciais, P., Dumas, P., Tang, Q., Wang, X., et al. (2020). Deceleration of China's human water use and its key drivers. *Proceedings of the National Academy of Sciences*, 117(14), 7702–7711. <https://doi.org/10.1073/pnas.1909902117>
- Zhou, W., Huang, G., Pickett, S. T., Wang, J., Cadenasso, M. L., McPhearson, T., et al. (2021). Urban tree canopy has greater cooling effects in socially vulnerable communities in the US. *One Earth*, 4(12), 1764–1775. <https://doi.org/10.1016/j.oneear.2021.11.010>
- Zitter, C. D., Pedersen, E. J., Kucharik, C. J., & Turner, M. G. (2019). Scale-dependent interactions between tree canopy cover and impervious surfaces reduce daytime urban heat during summer. *Proceedings of the National Academy of Sciences*, 116(15), 7575–7580. <https://doi.org/10.1073/pnas.1817561116>

References From the Supporting Information

- Betts, R. A. (2000). Offset of the potential carbon sink from boreal forestation by decreases in surface albedo. *Nature*, 408(6809), 187–190. <https://doi.org/10.1038/35041545>
- Chakraborty, T., Venter, Z. S., Qian, Y., & Lee, X. (2022). Lower urban humidity moderates outdoor heat stress. *AGU Advances*, 3(5), e2022AV000729. <https://doi.org/10.1029/2022AV000729>
- Florczyk, A. J., Melchiorri, M., Corbane, C., Schiavina, M., Maffenini, M., Pesaresi, M., et al. (2019). Description of the GHS Urban Centre Database 2015: Public release 2019: Version 1.0 [Dataset]. *JRC Publications Repository*. <https://doi.org/10.2760/037310>
- Gong, P., Li, X., Wang, J., Bai, Y., Chen, B., Hu, T., et al. (2020). Annual maps of global artificial impervious area (GAIA) between 1985 and 2018. *Remote Sensing of Environment*, 236, 111510. <https://doi.org/10.1016/j.rse.2019.111510>
- Gutman, G. G. (1999). On the monitoring of land surface temperatures with the NOAA/AVHRR: Removing the effect of satellite orbit drift. *International Journal of Remote Sensing*, 20(17), 3407–3413. <https://doi.org/10.1080/014311699211435>
- Lee, X., Goulden, M. L., Hollinger, D. Y., Barr, A., Black, T. A., Bohrer, G., et al. (2011). Observed increase in local cooling effect of deforestation at higher latitudes. *Nature*, 479(7373), 384–387. <https://doi.org/10.1038/nature10588>
- Li, X., & Zhou, Y. (2017). Urban mapping using DMSP/OLS stable night-time light: A review. *International Journal of Remote Sensing*, 38(21), 6030–6046. <https://doi.org/10.1080/01431161.2016.1274451>
- Middel, A., AlKhaled, S., Schneider, F. A., Hagen, B., & Coseo, P. (2021). 50 grades of shade. *Bulletin of the American Meteorological Society*, 102(9), E1805–E1820. <https://doi.org/10.1175/BAMS-D-20-0193.1>
- Yang, Q., Xu, Y., Wen, D., Hu, T., Chakraborty, T. C., Liu, Y., et al. (2024). Satellite clear-sky observations overestimate surface urban heat islands in humid cities. *Geophysical Research Letters*, 51(2), e2023GL106995. <https://doi.org/10.1029/2023GL106995>
- Zhang, T., Zhou, Y., Zhu, Z., Li, X., & Asrar, G. R. (2022). A global seamless 1 km resolution daily land surface temperature dataset (2003–2020). *Earth System Science Data*, 14(2), 651–664. <https://doi.org/10.5194/essd-14-651-2022>